

## RESEARCH ARTICLE

# Compact Self-Isolated Four-Element MIMO Antenna for WLAN and ISM Bands Application

**F. MOHSENFARD, A. MAHMOODZADEH, AND Z. ADELPOUR**

Department of Electrical Engineering, Shiraz Branch, Islamic Azad University, Shiraz 74731-71987, Iran

Corresponding author: A. Mahmoodzadeh (mahmoodzadeh@iaushiraz.ac.ir)

**ABSTRACT** A compact self-isolated four-element MIMO antenna is introduced for use in ISM systems and WLAN applications in the 2.4 GHz frequency band. The proposed design consists of four printed dipoles so four integrated baluns are responsible for feeding these antennas. By choosing an appropriate arrangement of the elements next to each other and using the feature of self-isolated antennas, great isolation is achieved in the first step. Finally, by utilizing a printed decoupling component in the space between the dipoles, the value of the envelope correlation coefficient (ECC) parameter comes very close to zero for the MIMO antenna. The major part of the isolation in this design is the responsibility of the self-isolated technique, and adding the decoupling element at the last stage of the design is to complete the antenna isolation process. The fabricated prototype of the proposed MIMO antenna operating at 2.25-2.87 GHz frequency band reaches the measured port-to-port isolation of better than 19 dB, ECC of less than 0.0009, the peak gain of 8.6 dBi with total dimensions of  $1.11\lambda_0 \times 1.11\lambda_0 \times 0.34\lambda_0$ . The numerical and experimental results approve the excellent MIMO performance for 2.4 GHz applications.

**INDEX TERMS** Self-isolated, MIMO antenna, WLAN, ISM.

## I. INTRODUCTION

In recent decades, with the need to increase the channel capacity and overcome the problem of multipath fading, MIMO antenna design has become more popular. The MIMO configurations have significantly improved the capacity and reliability of systems by making a different kind of diversity [1]. The MIMO antenna designers face two chief challenges: reducing the antenna size and creating adequate isolation between ports. Various techniques have been reported in the literature to eliminate mutual coupling between the antenna elements, such as optimization of the antenna geometries [2], metamaterial structure [3], decoupling network [4], [5], the dual-polarized antenna [6], the defected ground structure (DGS) [7] and [9], the neutralization line [10], [11], [12], and the multimode decoupling method [13]. Furthermore, a four-element MIMO antenna is introduced in [14] for sub-6 GHz 5G wireless applications. This antenna uses Split Ring Resonators (SRRs) to increase the antenna bandwidth. Also, by locating the

antenna elements at an appropriate electrical distance, port-to-port isolation and the ECC of the antenna become less than  $-15$  dB and 0.1, respectively. A printed MIMO dipole antenna with integrated baluns for WLAN applications at 2.4 GHz frequency is investigated in [15]. To improve the isolation between the adjacent elements, they are placed together in the perimeter of a square. In this configuration, the parallel elements are isolated with the same polarization by a sufficient distance. Oppositely, the orthogonal elements have different polarization, leading to proper isolation. Moreover, the mentioned antenna has an impedance bandwidth of 2.20-2.72 GHz, a peak gain of 8.37 dBi, isolation of less than  $-15$  dB, and ECC under 0.01. A microstrip line resonator of thickness 0.5 mm as a decoupling element decreases the mutual coupling between the ports [16]. One end of this resonator is opened, and the other side is shorted to the ground using a metallic via. This MIMO antenna operates at 2.2-12.3 GHz bandwidth with isolation of less than  $-16$  dB, and the ECC value is below 0.3. Furthermore, the use of the defected ground plane [17], employing the decoupling configurations between the antenna components, and using various slots and stubs on the ground plane are two popular

The associate editor coordinating the review of this manuscript and approving it for publication was Nagendra Prasad Pathak.

methods to increase the MIMO antenna isolation [18] and [19]. Also, other designs are presented in references [20], [21], [22], [23], [24], which have acceptable results. The last part of the paper compares the references mentioned with the proposed design in a table. The references mentioned above often follow two types of design. These antennas either have a planar structure like references [14] and [18], [19], [20], or they support a 3D configuration like references [15], [16], [17] and [21], [22], [23], [24]. Planar antennas usually have lower gain and isolation and can often show good gain and performance at higher frequencies. Nevertheless, regarding antennas with 3D configuration, it can be said that in these references, no effort has been made to improve the antenna's performance by investigating the arrangement of the radiation elements. Radiation elements in these references are often placed next to each other in the form of a cross-shaped or arranged in a square-shaped. In this paper, an attempt has been made to choose the best arrangement for antenna radiation elements by studying different topologies so that, in addition to creating excellent isolation between the elements, the space occupied by the antenna can be reduced as much as possible. By applying the methods mentioned earlier, the suitable performance of the MIMO antennas is overshadowed by increasing the dimension and complicating the structure of the antenna. On the other hand, the prominent feature of the self-isolated MIMO antennas without using additional elements or any external networks in the antenna structure is the preferred choice to solve this problem. In the configuration of the MIMO antennas with the self-isolated feature, the radiation elements located next to each other at a very short distance perform their function as an antenna and prevent the production fields from affecting each other simultaneously. Recently, some self-isolated antennas have been introduced that have not used additional elements to create sufficient isolation in these antennas [25] and [26]. A MIMO system using the antenna elements that have the self-isolated feature for the 5G applications is presented in [26]. The antenna is composed of a T-shaped feeding element and two identical L-shaped radiating elements positioned symmetrically. The L-shaped elements work as the radiating elements and act as a decoupling element between two neighboring radiating elements. In this design, Isolation > 20 dB for the presented structure is realized without any extra decoupling elements. Consequently, it is possible to design this antenna with compact dimensions. Furthermore, to reduce the weight of the antenna, the use of Printed Circuit Board (PCB) technology and the application of the dielectric substrates in their fabrication is recommended [15].

The self-isolated antenna characteristic is achieved by locating the antenna elements properly rather than using additional decoupling elements between them. The compact self-isolated four-element MIMO antenna reaches excellent isolation (ECC of less than 0.004) and good radiation performance. In the last phase, a planar printed decoupling component is used to reduce the mutual coupling of the antenna further. Finally, a self-isolated MIMO antenna with

an operating frequency band of 2.25-2.87 GHz and measured port-to-port isolation of better than 19 dB and ECC of less than 0.0009 is achieved.

## II. DIPOLE ANTENNA ELEMENT DESIGN

Since the dipole is a balanced element, while the coaxial cable is an unbalanced transmission line, directly feeding the dipole antenna with the coaxial cable can reduce the antenna's performance. A balun is a device that turns an unbalanced transmission line into a balanced one. One of the most widely used baluns employed in dipoles is the  $\lambda/4$  coaxial balun. In 2009, a printed model of this balun was introduced and the integrated balun was named, which is used in this article [27]. The  $\lambda/4$  coaxial balun has a 3D structure, so the balun part is placed next to the coaxial cable and soldered. However, in the integrated balun configuration, the entire structure is placed on the printed circuit board, and its various components are united. The integrated balun consists of three general parts. The first portion of the balun consists of a vertical  $\Gamma$ -shaped feeding part and a short-circuited plane behind it, which together form a tapered microstrip line and receive the signal from the coaxial cable. The horizontal part of the  $\Gamma$ -shaped feed line and the middle gap between the two short-circuited planes are an essential part of the balun, which forms a slot line, and the signal is coupled to the dipole and transmitted through it. This part is the second portion of the balun. Finally, a small vertical part of the  $\Gamma$ -shaped feed with a short-circuited plane forms the third portion of the balun, which is responsible for matching the impedance of the feeding line and enhancing the electromagnetic coupling. The overall structure of the proposed dipole antenna element is demonstrated in Fig. 1. The introduced dipole antenna involves two FR-4 substrates with a thickness of 0.8 mm, a relative permittivity of 4.4, and a loss tangent of 0.02. One of these substrates, with dimensions of  $40 \times 60 \text{ mm}^2$  (Substrate-1), which includes dipole arms and integrated balun, is placed vertically on the other substrate, with dimensions of  $113 \times 113 \text{ mm}^2$  (Substrate-2), which is the ground of the antenna. The dipole arms are printed on the vertical substrate, and the integrated balun structure is printed on the contrary side of this substrate.

The horizontal substrate is covered with conductive plates to shorten the vertical stubs of the balun and connect the SMA to the antenna. A 3D view, a front view, and a side view of the printed dipole antenna element are displayed in Fig.1 (a), (b), and (c), respectively. It can be seen that the integrated balun structure consists of a  $\Gamma$ -shaped feed and a slot-line, which is short-circuited at the end. In this configuration, the dipole length is denoted by  $L_d$ , which plays a significant role in determining the resonant frequency of the dipole antenna.

In the proposed structure, a coaxial cable is responsible for feeding the antenna so that an SMA is connected to it from the back of the horizontal substrate. In this way, the SMA outer conductor is soldered to the horizontal substrate back-plate, and the SMA inner conductor is soldered to the

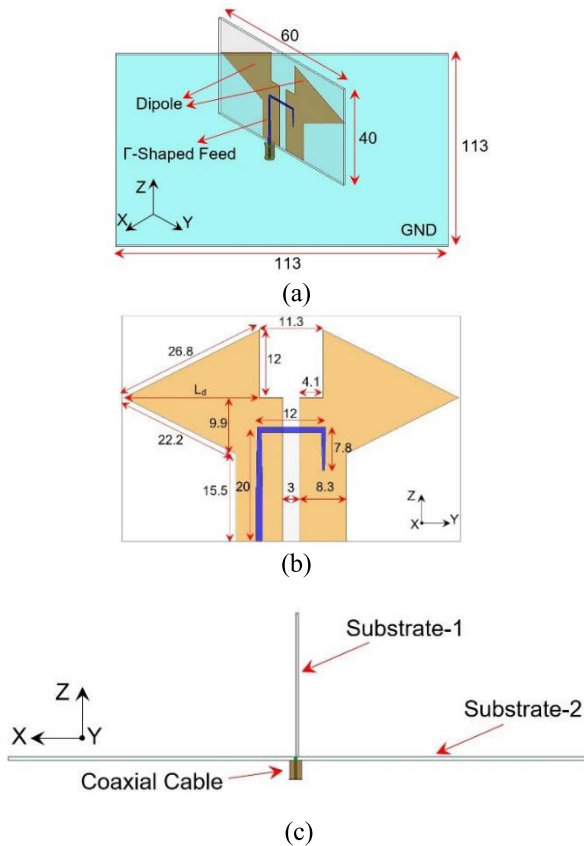


**FIGURE 1.** Configuration of the patch antenna (a) at front- and -side views and (b) at the 3D view (All dimensions are in millimeters, mm).

Γ-shaped feed via a hole. It should be noted that the balun used in this design consists of three parts. The first part of the balun, connected to the SMA connector, is a microstrip line, which receives the input power via the coaxial cable. The next part consists of a horizontal stub that is the excitation point of this antenna and can stimulate a slot line by electromagnetic coupling. The slot line reaches the dipole arms at the top of its path and is short-circuited at the bottom of its path at the end. The third part of the balun structure involves an open-circuited microstrip line, which is responsible for making an appropriate impedance matching. Applying the balun can improve the impedance matching and reduce its cross-polarization level. The simulated  $S_{11}$  response and radiation efficiency of the proposed dipole antenna element are shown in Fig. 2.

It can be seen that the impedance bandwidth for the  $-10$  dB specification is 19.6% (2.26–2.75 GHz), which covers the operating frequency band of WLAN (2.4–2.48 GHz) and ISM (2.4–2.5 GHz) systems. Also, the radiation efficiency of the dipole antenna is more than 85% in the operating frequency band. A parametric study was also performed on the length of the dipole arms ( $L_d$ ). The results of this analysis are shown in Fig. 3. According to the results, it is observed that as the length of the dipole arms increases from 14 mm to

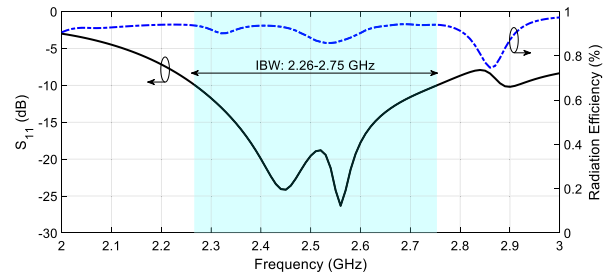


**FIGURE 2.** Numerical  $|S_{11}|$  and radiation efficiency of the proposed dipole antenna element.

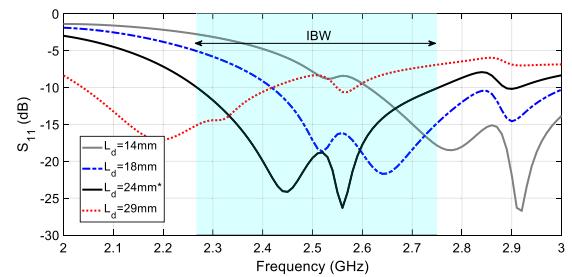


**FIGURE 3.**  $|S_{11}|$  response as a function of the dipole arms ( $L_d$ ).

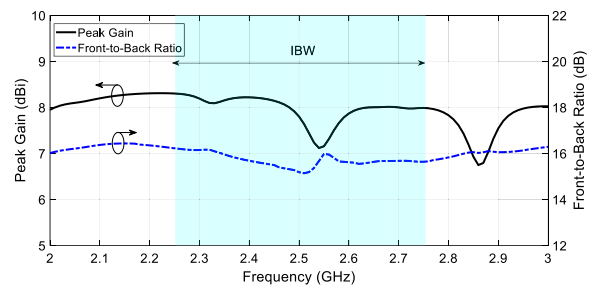


**FIGURE 4.** Numerical gain and FBR of the dipole antenna element.

29 mm, the resonance frequency of the structure decreases from 2.91 GHz to 2.18 GHz. Therefore, by adjusting the  $L_d$  at 24 mm, a resonance frequency is obtained for the antenna at 2.45 GHz. The gain diagram and Front-To-Back Ratio (FBR) curve of the proposed dipole antenna element are shown in Fig. 4. Obviously, this design has an average gain and FBR of approximately 8 dB and 16 dB in the operating frequency range, correspondingly. It must be emphasized that the gain and FBR values of the dipole are calculated in the  $+Z$  direction.

Fig. 5 shows the dipole antenna’s H-plane and E-plane normalized radiation patterns. Consequently, stable unidirectional radiation is achieved in the  $+Z$  direction.

The patterns also show that the X-pol radiation in both planes is under  $-25$  dB in the operating frequency due to using the balun structure to feed the proposed antenna. Furthermore, the half-power beamwidth (HPBW) is  $85.5^\circ$  in the H-plane and  $54.7^\circ$  in the E-plane at 2.45 GHz.

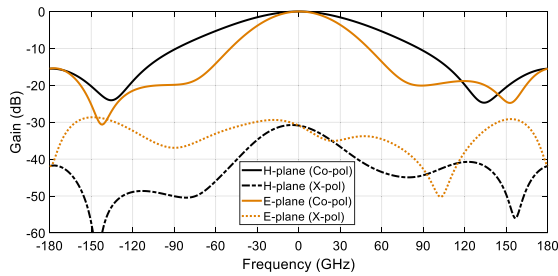


**FIGURE 5.** Numerical normalized patterns of the dipole antenna element at 2.45 GHz: (a) H-plane (xz-plane) and (b) E-plane (yz-plane).

### III. MIMO ANTENNA DESIGN

The main goal of this paper is to reduce the space occupied by the antenna. As it is known, reducing the space occupied by the antenna in any wireless telecommunication system reduces the overall dimensions of the system and thus reduces its cost. On the other hand, according to Shannon’s Law, the channel’s capacity is directly proportional to the number of elements of the MIMO system. The channel capacity can also be increased by increasing the number of MIMO antenna elements. Furthermore, the problem of multipath fading is solved with MIMO antennas. The antenna designed in this paper is for ISM and WLAN applications, in both of which the effort to reduce the dimensions of the system is appreciated and justified. One of the ways to reduce mutual coupling in MIMO antennas is to use spatial diversity. However, this technique can significantly increase the dimensions of the MIMO antenna system. Therefore, in the first step, the MIMO antenna elements should be placed next to each other so that in addition to reducing the dimensions of the antenna, it also creates sufficient isolation. Therefore, the self-isolated technique seems very useful in this design. In addition to paying attention to the different parameters of the antenna (bandwidth, gain, radiation pattern, etc.) in this design, with the analysis and investigations, the best way for the arrangement of MIMO antenna elements has been obtained, so that it results in high insulation with little wasted space. Four printed dipole antenna elements located close to each other are used in designing the self-isolated MIMO antenna in this study. The primary purpose of this paper is to choose an appropriate arrangement for the four radiation elements so that the elements can prevent the destructive effect of the fields on each other’s performance in addition to performing their principal task of creating the radiation field. Consequently, the property of the self-isolated antenna is achieved so that sufficient isolation between the elements is realized without additional elements. According to Fig. 6, three different states are provided for the configuration of the MIMO antenna, which comprises four radiation elements next to each other to obtain intended isolation between them. In addition to using this feature, a decoupling component is located in the space in the middle of the MIMO structure in the third state to prevent the mutual coupling between the dipoles completely. In state-1 of the MIMO antenna configuration, the dipole

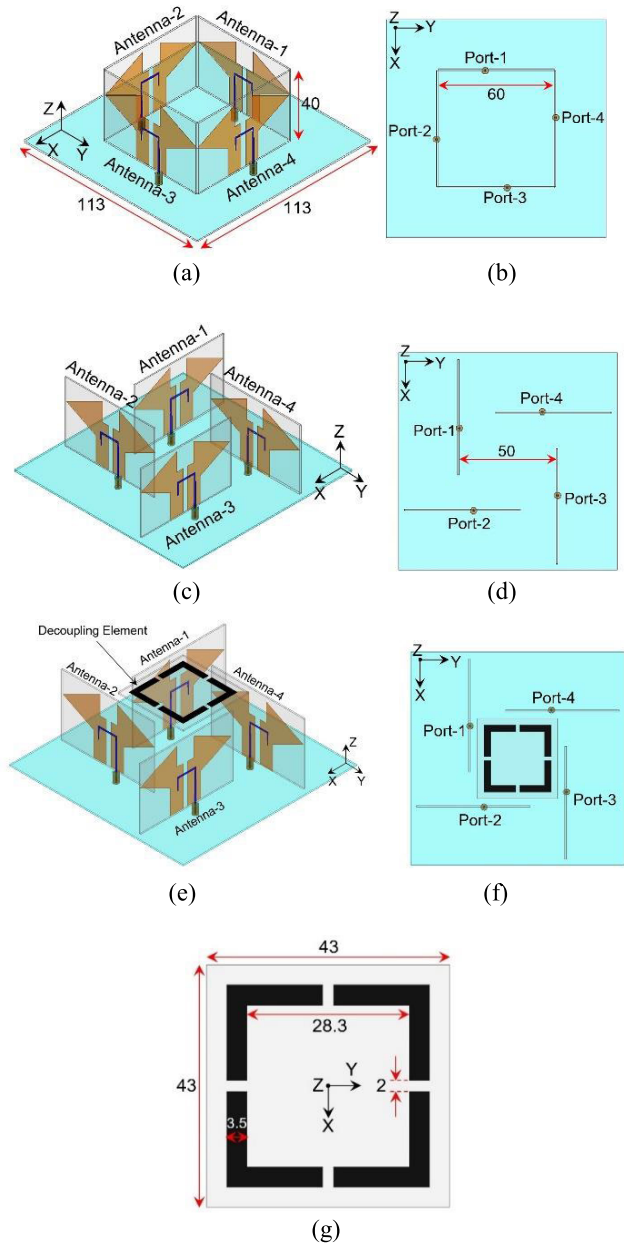


**FIGURE 6.** 3D view, and top view of the configuration of the MIMO antenna in (a) and (b) state-1, (c) and (d) state-2, (e) and (f) state-3, and (g) geometry of the decoupling element.

antenna elements are located around each other in a square environment. Considering the achievement of high isolation and compact dimensions, this is the simplest way to put four dipole antennas together. In this way, the antennas are in two positions relative to each other, either orthogonal or parallel, so in the isolation analysis of the MIMO antenna, these two types of placement will be considered. Fig. 6 (a) and (b) show the antenna structure in state-1. The dimensions and type of substrates used in this state are similar to the dipole antenna element’s configuration. The antenna height in this state is 40 mm, and the horizontal and vertical distance of the elements from each other is 60 mm. In state-2, the arrangement

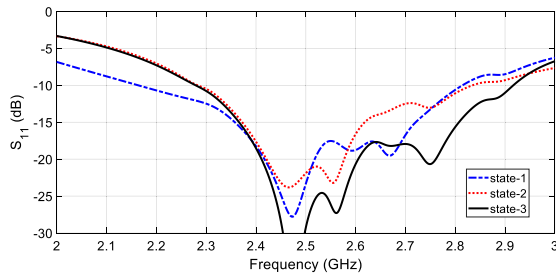


**FIGURE 7.** Numerical  $|S_{11}|$  of the proposed MIMO antenna in states-1 to -3.

of dipole elements is formed by rotating the antenna elements at  $45^\circ$ . The self-isolated MIMO antenna structure in state-2 is presented in Fig. 6 (c) and (d). In this configuration, the ground plane is rotated  $45^\circ$ , like the antenna elements, and the optimized structure of the MIMO antenna is formed with the self-isolated feature. The ground plane is placed more appropriately under the MIMO antenna elements in this arrangement. In the last stage of MIMO antenna design, a decoupling element has been added to complete the isolation process. In state-3, a combined technique is used to suppress the mutual coupling between the elements in the proposed MIMO antenna design. In addition to using the feature of self-isolated antenna, a decoupling element is employed as a complement to the isolation process. The geometry of the antenna and decoupling element in state-3 is demonstrated in Fig. 6 (e) and (f). The employed decoupling element consists of four L-shaped stubs forming a ring together. Regarding Fig. 6 (g), each of the L-shaped arms is positioned between two radiation elements, which reduces the mutual coupling between the antenna components.

The numerical scattering parameters for the MIMO antenna in states-1 to -3 are exposed in Fig. 7. Due to the structural symmetry of the MIMO antenna, the results related to the bandwidth of the MIMO antenna are reported only for port-1. According to the results, the presented configuration in state-1 has a wide operating frequency range of 2.16–2.81 GHz. It is found that the impedance bandwidth of the MIMO antenna in state-1 is almost similar to the bandwidth of the dipole antenna element. Similar results have been obtained in states-2 and -3. The proposed MIMO antenna has an impedance bandwidth of 2.28–2.84 GHz and 2.28 to 2.91 GHz in states-2 and -3, respectively. It is clear that the arrangement of the antenna elements and even the presence of the decoupling element do not significantly affect the antenna's impedance bandwidth.

Also, the results related to the isolation of the MIMO antenna between parallel and orthogonal elements are displayed in Fig. 8 (a) for states-1 to -3. According to the results, the parallel elements in state-1 have isolation higher than 14 dB. The isolation of vertical elements approximately comes close to  $-10$  dB. This indicates that the MIMO antenna isolation is not suitable in state-1. Therefore, reconsidering the configuration of the presented MIMO antenna

seems necessary. Furthermore, the outcomes of the ECC parameter of the MIMO antenna in states-1 to -3 are demonstrated in Fig. 8 (b) between the orthogonal and parallel elements. The value of this parameter for state-1 is less than 0.005. The results obtained in the first state showed that the introduced configuration could not satisfactorily meet the requirements of the MIMO systems, so the configuration of state-2 for the MIMO antenna is proposed. This configuration, using the feature of the self-isolated antenna, gives worthy results for the MIMO antenna. In this arrangement, the location of the antenna ports and the total dimension of the antenna compared to the previous state have been preserved. By rotating the radiation elements and ground plane in state-2 configuration, the dipole arms, and in particular the  $\Gamma$ -shaped feed, are placed opposite each other less than in state-1, and it is expected that in this case, the antenna isolation will improve. However, the direct distance of dipole antenna elements in state-2 is less than in state-1 (50 mm). The simulated isolation and ECC parameter for the self-isolated MIMO antenna are shown in Fig. 8. The results approve that the isolation between the parallel elements and the orthogonal elements is more than 23 and 17 dB, respectively. Also, the ECC value of the self-isolated MIMO antenna is less than 0.004. The ECC parameter in this study is calculated from the S-parameters using the following equation [18].

$$ECC = \frac{|S_{ii}^* S_{ij} + S_{ji}^* S_{jj}|^2}{(1 - (|S_{ii}|^2 + |S_{jj}|^2)) (1 - (|S_{jj}|^2 + |S_{ii}|^2))} \quad (1)$$

where the  $S_{ii}$  is the reflection coefficient of the antenna (i) and  $S_{ij}$  (with  $i \neq j$ ), is the transmission coefficient between the antenna (i) and the antenna (j).

According to the results, the design presented in state-3 has isolation above 19 dB in most of the frequency band. Also, the ECC values of this antenna are less than 0.002. The results approve that the presented MIMO antenna in state-3 is had better isolation by using the decoupling element. Furthermore, the gain and FBR curves in states-1 to -3 are illustrated in Fig. 9 for one of the antenna ports (port-1). The gain and FBR at other ports are not shown because the four antenna elements are symmetrical. The H-plane and E-plane normalized patterns in states-1 to -3 are displayed in Fig. 10 for one port. Regarding the plotted radiation patterns, stable unidirectional radiation in the  $\varphi = 0^\circ$  and  $\theta = 0^\circ$  direction is achieved. In addition, the X-pol radiation in both planes are under  $-10$  dB in the operating frequency band. The results show that the antenna gain reduction and FBR fluctuations are compensated in state-2. Consequently, in state-2 of the self-isolated MIMO antenna design, the antenna radiation properties are improved and the antenna isolation values are acceptable. Therefore the self-isolated MIMO antenna design is accomplished in state-2. Also it can be seen that the proposed MIMO antenna in state-3 has an average gain

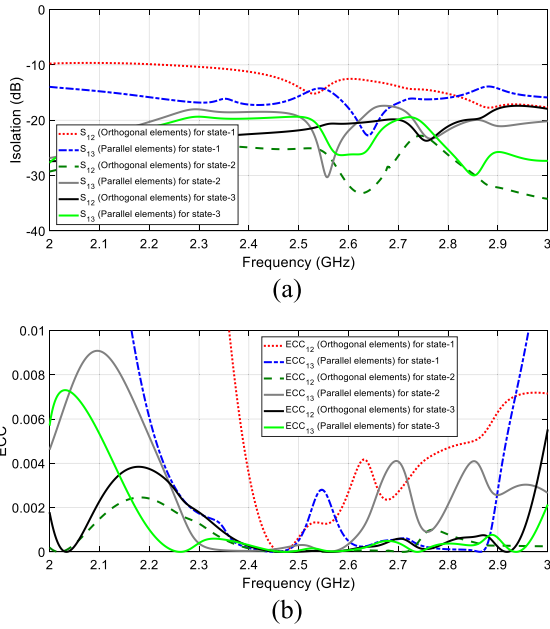


FIGURE 8. Numerical (a) isolation and (b) ECC parameters of the proposed MIMO antenna at orthogonal and parallel elements in states-1 to -3.

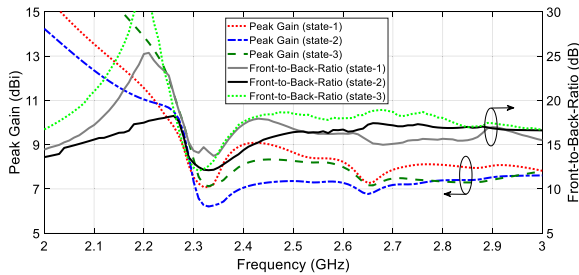


FIGURE 9. Numerical gain and FBR of the MIMO antenna in states-1 to -3 at port-1.

of 7.75 dB in its frequency band, and a maximum value of 19 dB has been reported for the FBR parameter.

The dispersion diagram for the decoupling structure over the Brillouin zone ( $\Gamma$ -X-M- $\Gamma$ ) is plotted in Fig. 11 to better understand how it works.

It is observed that the fundamental mode curve of the signal is under the light line curve and approves that the EM wave cannot pass through the decoupling element in the x- and y-direction over the frequency band of 2.45-3.1 GHz. On the other hand, the curve plotted in Fig. 11 is in the slow-wave region [28]. Furthermore, the surface current density comparison between state-1 and state-3 is demonstrated in Fig. 12 to show the improvement of the port isolation. In this figure, it is clear that by exciting port-1 of the MIMO antenna, its effect on the other ports is reduced by the presence of the decoupling element.

IV. ANTENNA FABRICATION AND MEASUREMENT

Fig. 13 exhibits photos of the prototype of the proposed MIMO antenna. The proposed MIMO antenna was fabricated

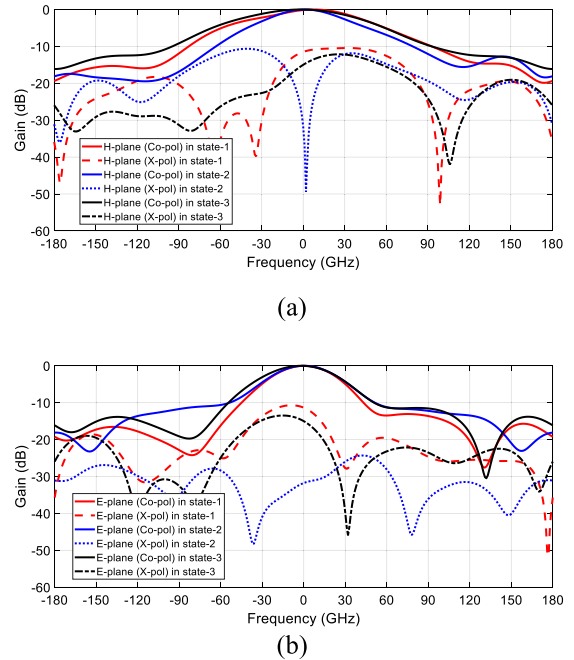


FIGURE 10. Numerical normalized patterns of the MIMO antenna in states-1 to -3 at port-1: (a) H-plane (yz-plane), and (b) E-plane (xz-plane) at 2.45 GHz.

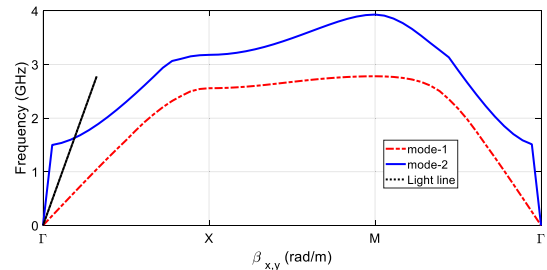


FIGURE 11. Dispersion diagram of incident wave on the decoupling element.

using FR-4 substrates after optimization steps and was tested and measured in the antenna laboratory by a Vector Network Analyzer (VNA) of the Agilent-8363C type. Fig. 13 also displays the proposed antenna testing process in the antenna laboratory. The used substrates and the assembled proposed antenna are shown in Fig. 13 (a) and (b), respectively. Furthermore, two photos of the test process are shown in Fig. 13 (c) and (d).

The experimental results of the proposed MIMO antenna are shown in Fig. 14 to Fig. 17. The results show that the fabricated prototype has an operating frequency band of 2.25-2.87 GHz, measured port-port isolation above 19 dB, ECC of less than 0.0009, and a peak gain of 8.6 dBi with total dimensions of  $1.11\lambda_0 \times 1.11\lambda_0 \times 0.34\lambda_0$ , where  $\lambda_0$  corresponds to the free space wavelength at the center frequency of the antenna impedance bandwidth. The numerical and experimental results are very similar, which shows that the simulations have been validated. The H-plane and

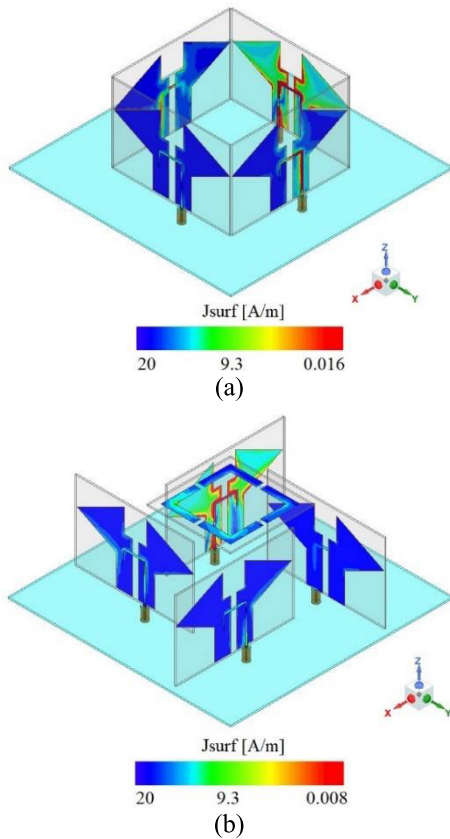


FIGURE 12. Surface current density ( $J_{surf}$ ) at 2.5 GHz for MIMO antenna in (a) states-1, and (b) states-3 by exciting port-1.

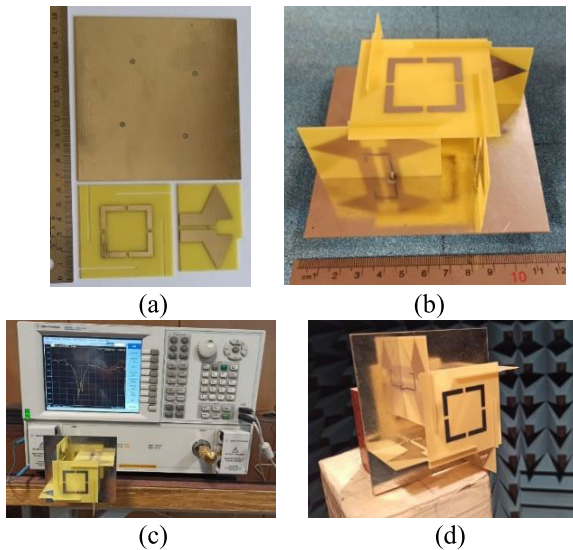


FIGURE 13. Photographs of the fabricated proposed MIMO antenna: (a) unassembled and (b) assembled antenna, (c) measure S-parameters of the antenna, and (d) measurement of the antenna radiation parameters.

E-plane normalized patterns are plotted in Fig. 17. Stable unidirectional radiation in the  $\varphi = 0^\circ$  and  $\theta = 0^\circ$  direction is observed from the antenna.

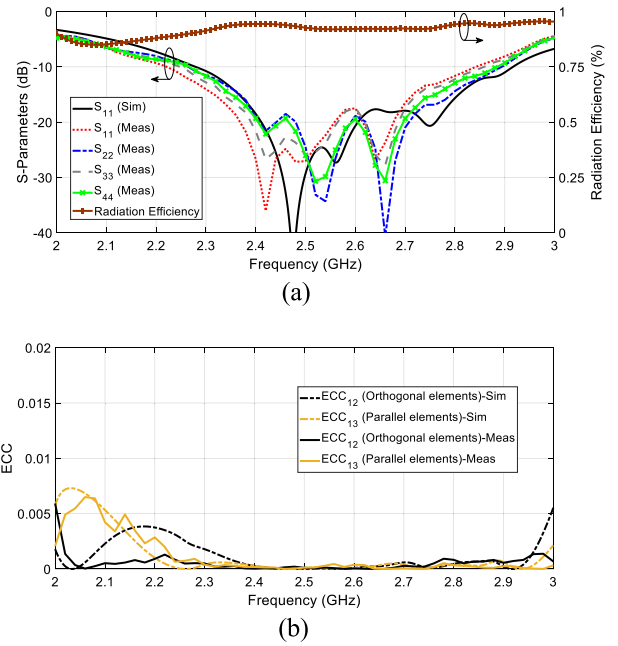


FIGURE 14. Numerical and experimental S-parameters for the proposed MIMO antenna: (a) return loss and radiation efficiency, and (b) isolation.

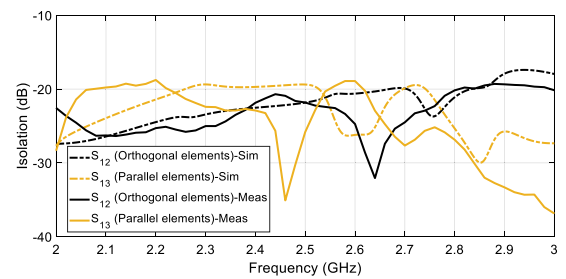


FIGURE 15. Numerical and tested ECC parameters.

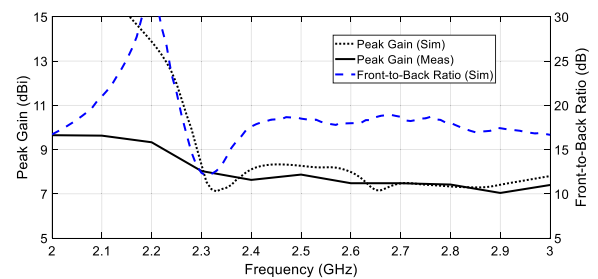
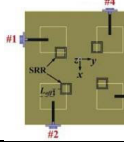
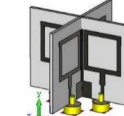
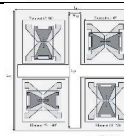
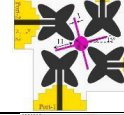
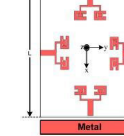
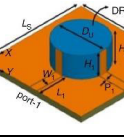
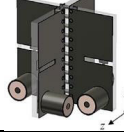


FIGURE 16. Numerical and experimental gain and simulated FBR at port-1.

Measured radiation patterns show that the Cross-polarization level is at least 10 dB lower than the Co-polarization. Moreover, the HPBW of the proposed MIMO antenna is  $97.1^\circ$  in the H-plane and  $51.4^\circ$  in the E-plane at 2.45 GHz. The antenna results are compared with some four-element MIMO antennas in Table 1. According to the results mentioned in the comparison table, the proposed antenna, considering the dimensions, provides the best

TABLE 1. Comparison of the proposed antenna with some four-element MIMO antennas.

Ref.	IBW [GHz]	Isolation [dB]	ECC	Gain [dBi]	Size [ $\lambda_0^3$ ]	Antennas Position
[14]	3.56-4	>15	<0.1	2.39	$0.76 \times 0.76 \times 0.01$ $=0.005776$	
[15]	2.20-2.72	>15	<0.01	8.37	$1.31 \times 1.31 \times 0.2$ $=0.343220$	
[16]	2.2-12.3	>16	<0.3	5.52	$0.63 \times 0.63 \times 0.41$ $=0.162729$	
[17]	2.38-2.58 3.20-5.96	>10	<0.00015	4.8 9.2	$6.63 \times 6.63 \times 1.1$ $=48.35259$	
[18]	7.58-8.04 9.23-10.79	>20	<0.003 <0.005	2.5	$1.22 \times 1.22 \times 0.08$ $=0.119072$	
[19]	2.16-3.20	>21.4	<0.001 <0.0004	0.68	$0.63 \times 0.63 \times 0.01$ $=0.003969$	
[20]	25.5-29.6	>17	<0.01	8.3	$2.75 \times 3.21 \times 0.07$ $=0.617925$	
[21]	5.4-6.0	>18	<0.25	5	$0.57 \times 0.57 \times 0.26$ $=0.084474$	
[22]	2.8-9.50	>15	<0.1	5.41	$0.66 \times 0.31 \times 0.66$ $=0.135036$	
[23]	3.0-20.0	>20	<0.1	5.0	$1.69 \times 1.69 \times 1.92$ $=5.483712$	
[24]	3.0-6.75	>15	<0.1	4.97	$0.32 \times 0.39 \times 0.39$ $=0.048672$	
This Work	2.25-2.87	>19.3 >19	<0.0009 <0.0005	8.6	$1.11 \times 1.11 \times 0.34$ $=0.418914$	



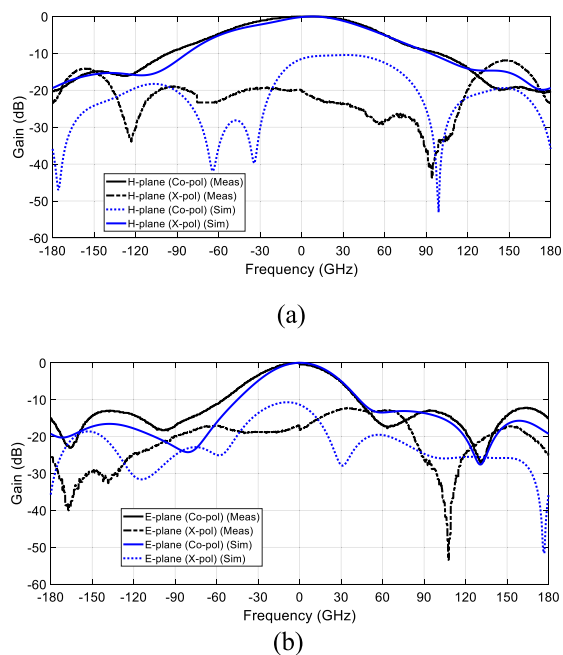


**FIGURE 17. Numerical and experimental normalized patterns of the proposed MIMO antenna: (a) xz-plane and (b) yz-plane at 2.45 GHz and port-1.**

isolation and the highest gain. In fact, our main contribution in this paper is to improve the parameters of the antenna with the most compact dimensions by discussing how to arrange the MIMO antenna elements.

**V. CONCLUSION**

A new structure of MIMO antenna is introduced that uses four printed dipoles, a ground panel, and a decoupling element in this study. This study’s main contribution is using two combined methods to suppress the mutual coupling. By investigating and analyzing the different arrangements of dipole elements next to each other, a configuration was obtained that could create the self-isolated feature in the antenna. The self-isolated MIMO antenna achieved good isolation and radiation properties. In the second design step, a decoupling element was also applied between the antenna radiation elements in addition to using the self-isolated feature to increase the antenna isolation. The practical results show that the fabricated antenna is a good candidate for ISM Band and WLAN Applications at the operating frequency of 2.4 GHz.

**REFERENCES**

[1] B. Niu and J. Tan, “Compact self-isolated MIMO antenna system based on quarter-mode SIW cavity,” *Electron. Lett.*, vol. 55, no. 10, pp. 574–576, May 2019.

[2] S. Yan, P. J. Soh, and G. A. E. Vandenbosch, “Dual-band textile MIMO antenna based on substrate-integrated waveguide (SIW) technology,” *IEEE Trans. Antennas Propag.*, vol. 63, no. 11, pp. 4640–4647, Nov. 2015.

[3] G. Zhai, Z. N. Chen, and X. Qing, “Enhanced isolation of a closely spaced four-element MIMO antenna system using metamaterial mushroom,” *IEEE Trans. Antennas Propag.*, vol. 63, no. 8, pp. 3362–3370, Aug. 2015.

[4] C.-H. Wu, C.-L. Chiu, and T.-G. Ma, “Very compact fully lumped decoupling network for a coupled two-element array,” *IEEE Antennas Wireless Propag. Lett.*, vol. 15, pp. 158–161, 2016.

[5] K. Qian, L. Zhao, and K.-L. Wu, “An LTCC coupled resonator decoupling network for two antennas,” *IEEE Trans. Microw. Theory Techn.*, vol. 63, no. 10, pp. 3199–3207, Oct. 2015.

[6] S. Gao, L. W. Li, M. S. Leong, and T. S. Yeo, “A broad-band dual-polarized microstrip patch antenna with aperture coupling,” *IEEE Trans. Antennas Propag.*, vol. 51, no. 4, pp. 898–900, Apr. 2003.

[7] C.-Y. Chiu, C.-H. Cheng, R. D. Murch, and C. R. Rowell, “Reduction of mutual coupling between closely-packed antenna elements,” *IEEE Trans. Antennas Propag.*, vol. 55, no. 6, pp. 1732–1738, Jun. 2007.

[8] S. Shoaib, I. Shoaib, N. Shoaib, X. Chen, and C. G. Parini, “Design and performance study of a dual-element multiband printed monopole antenna array for MIMO terminals,” *IEEE Antennas Wireless Propag. Lett.*, vol. 13, pp. 329–332, 2014.

[9] S. Zhang, S. Khan, and S. He, “Reducing mutual coupling for an extremely closely-packed tunable dual-element PIFA array through a resonant slot antenna formed in-between,” *IEEE Trans. Antennas Propag.*, vol. 58, no. 8, pp. 2771–2776, Aug. 2010.

[10] S.-W. Su, C.-T. Lee, and F.-S. Chang, “Printed MIMO-antenna system using neutralization-line technique for wireless USB-dongle applications,” *IEEE Trans. Antennas Propag.*, vol. 60, no. 2, pp. 456–463, Feb. 2012.

[11] S. Wang and Z. Du, “Decoupled dual-antenna system using crossed neutralization lines for LTE/WWAN smartphone applications,” *IEEE Antennas Wireless Propag. Lett.*, vol. 14, pp. 523–526, 2015.

[12] A. Cihangir, F. Ferrero, G. Jacquemod, P. Brachat, and C. Luxey, “Neutralized coupling elements for MIMO operation in 4G mobile terminals,” *IEEE Antennas Wireless Propag. Lett.*, vol. 13, pp. 141–144, 2014.

[13] H. Xu, H. Zhou, S. Gao, H. Wang, and Y. Cheng, “Multimode decoupling technique with independent tuning characteristic for mobile terminals,” *IEEE Trans. Antennas Propag.*, vol. 65, no. 12, pp. 6739–6751, Dec. 2017.

[14] D. Sarkar and K. V. Srivastava, “Four element dual-band sub-6 GHz 5G MIMO antenna using SRR-loaded slot-loops,” in *Proc. 5th IEEE Uttar Pradesh Sect. Int. Conf. Electr., Electron. Comput. Eng. (UPCON)*, Nov. 2018, pp. 1–5.

[15] R. Nasirzade, J. Nourinia, C. Ghobadi, M. Shokri, and R. Naderali, “Broadband printed MIMO dipole antenna for 2.4 GHz WLAN applications,” *J. Instrum.*, vol. 15, no. 1, Jan. 2020, Art. no. P01001.

[16] J. Premalatha and D. Sheela, “Compact four-port vertically polarized UWB monopole antenna for MIMO communications,” *Circuit World*, vol. 47, no. 2, pp. 129–137, Jun. 2021.

[17] B. Feng, J. Zhu, L. Deng, W. An, and Q. Zeng, “A printed dual-wideband magneto-electric dipole antenna and its MIMO system for WLAN and WiMAX applications,” in *Proc. IEEE Int. Conf. Comput. Electromagn. (ICCEM)*, Feb. 2016, pp. 256–258.

[18] A. Eslami, J. Nourinia, C. Ghobadi, and M. Shokri, “Four-element MIMO antenna for X-band applications,” *Int. J. Microw. Wireless Technol.*, vol. 13, no. 8, pp. 859–866, Oct. 2021.

[19] K. Kaboutari and V. Hosseini, “A compact 4-element printed planar MIMO antenna system with isolation enhancement for ISM band operation,” *AEU-Int. J. Electron. Commun.*, vol. 134, May 2021, Art. no. 153687.

[20] M. Khalid, S. I. Naqvi, N. Hussain, M. Rahman, S. S. Mirjavadi, M. J. Khan, and Y. Amin, “4-port MIMO antenna with defected ground structure for 5G millimeter wave applications,” *Electronics*, vol. 9, no. 1, p. 71, Jan. 2020.

[21] G. Das, A. Sharma, R. K. Gangwar, and M. S. Sharawi, “Compact back-to-back DRA-based four-port MIMO antenna system with bi-directional diversity,” *Electron. Lett.*, vol. 54, no. 14, pp. 884–886, Jul. 2018.

[22] M. Saravanan, R. Kalidoss, B. Partibane, and K. S. Vishvakshnan, “Design of an interlocked four-port MIMO antenna for UWB automotive communications,” *Int. J. Microw. Wireless Technol.*, vol. 14, no. 2, pp. 239–246, Mar. 2021.

[23] K. Srivastava, B. K. Kanaujia, S. Dwari, S. Kumar, and T. Khan, “3D cuboidal design MIMO/diversity antenna with band notched characteristics,” *AEU-Int. J. Electron. Commun.*, vol. 108, pp. 141–147, Aug. 2019.

[24] P. Bactavatchalame and K. Rajakani, “Compact broadband slot-based MIMO antenna array for vehicular environment,” *Microw. Opt. Technol. Lett.*, vol. 62, no. 5, pp. 2024–2032, May 2020.

[25] A. Zhao and Z. Ren, “Size reduction of self-isolated MIMO antenna system for 5G mobile phone applications,” *IEEE Antennas Wireless Propag. Lett.*, vol. 18, no. 1, pp. 152–156, Nov. 2019.

- [26] A. Zhao and Z. Ren, "Multiple-input and multiple-output antenna system with self-isolated antenna element for fifth-generation mobile terminals," *Microw. Opt. Technol. Lett.*, vol. 61, no. 1, pp. 20–27, Jan. 2019.
- [27] R. L. Li, T. Wu, B. Pan, K. Lim, J. Laskar, and M. M. Tentzeris, "Equivalent-circuit analysis of a broadband printed dipole with adjusted integrated balun and an array for base station applications," *IEEE Trans. Antennas Propag.*, vol. 57, no. 7, pp. 2180–2184, Jul. 2009.
- [28] N. Jaglan and S. D. Gupta, "Reflection phase characteristics of EBG structures and WLAN band notched circular monopole antenna design," *Int. J. Commun. Antenna Propag.*, vol. 5, no. 4, p. 233, Aug. 2015.



**A. MAHMOODZADEH** received the B.Sc. degree in electrical engineering from the University of Shiraz, in 2005, the M.Sc. degree in electrical engineering from the University of Shahed, in 2008, and the Ph.D. degree in electrical engineering from the University of Yazd, Iran, in 2013. Since 2009, she has been with Islamic Azad University, Shiraz Branch, Shiraz, Iran. Her research interests include pattern recognition and image and signal processing.



**F. MOHSENI FARD** was born in Talheh, Boushehr, Iran, in 1981. He received the B.Sc. and M.Sc. degrees in telecommunication engineering from Islamic Azad University of Boushehr Branch, Boushehr, in 2000 and 2006, respectively. He is currently pursuing the Ph.D. degree in communication engineering with Islamic Azad University, Shiraz Branch, Shiraz, Iran. He has been a Faculty Member of the Islamic Azad University of Khormuj, Khormuj, Iran, since 2010. His research interests include antenna design, microwave technology, instruments, electrical, fiber optics, and microwave filters.



**Z. ADELPOUR** received the B.Sc. and M.Sc. degrees in telecommunication engineering from Shiraz University, Shiraz, Iran, in 2006 and 2010, respectively, and the Ph.D. degree from the Amirkabir University of Technology, Tehran, Iran, in 2015. She is currently an Assistant Professor at the Shiraz Branch of Islamic Azad University, Shiraz. Her research interests include microwave technology, antenna design, nano-optics and nano-photonics, plasmonic devices, and nonlinear optics.

...